

See discussions, stats, and author profiles for this publication at: <https://www.researchgate.net/publication/280141449>

Solvent Influence on Thickness, Composition, and Morphology Variation with Dip-Coating Rate in Supramolecular PS-b-P4VP Thin Films

ARTICLE in MACROMOLECULES · JULY 2015

Impact Factor: 5.8 · DOI: 10.1021/acs.macromol.5b00847

CITATIONS

2

READS

14

7 AUTHORS, INCLUDING:



[Sébastien Roland](#)

MINES ParisTech

8 PUBLICATIONS 51 CITATIONS

[SEE PROFILE](#)

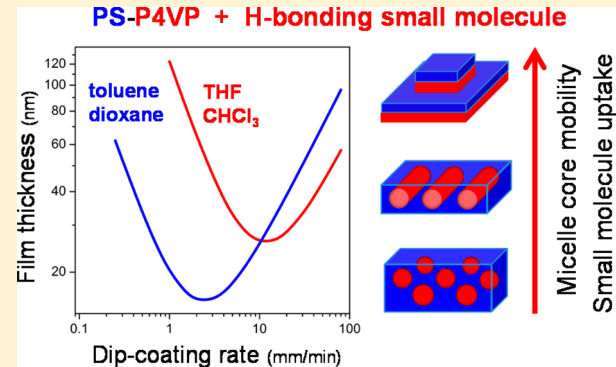
Solvent Influence on Thickness, Composition, and Morphology Variation with Dip-Coating Rate in Supramolecular PS-*b*-P4VP Thin Films

Sébastien Roland, Cé Guinto Gamys, Josué Grosrenaud, Stéphanie Boissé, Christian Pellerin,* Robert E. Prud'homme,* and C. Geraldine Bazuin*

Département de chimie, Centre de recherche sur les matériaux auto-assemblés (CRMAA/CSACS), Université de Montréal, C.P. 6128 Succ. Centre-ville, Montréal, QC, Canada H3C 3J7

Supporting Information

ABSTRACT: Recent literature has shown that the thickness of dip-coated films has a V-shaped dependence on dip-coating rate when very slow rates are included. For supramolecular block copolymer films, small molecule (SM) uptake and film morphology are also rate-dependent, as shown previously for a poly(styrene-*b*-4-vinylpyridine) (PS-P4VP) block copolymer in THF solutions containing naphthol (NOH) and naphthoic acid (NCOOH). Here, these investigations are extended to *p*-dioxane, toluene, and CHCl₃ solutions. The V-shaped thickness dependence is validated for each solvent, but with the V minimum displaced to lower dip-coating rates and thicknesses for the solvents with lower vapor pressures (*p*-dioxane, toluene), thereby decreasing the dip-coating rate range of the “capillarity regime” (slow side of the V) and consequently extending that of the “draining regime” (fast side of the V). The SM/VP uptake ratio varies with the nature of the solvent, particularly in the capillarity regime, where it is higher for solvents that are weak SM-VP hydrogen-bond competitors (toluene, CHCl₃). The draining regime generally shows greater SM uptake than the capillarity regime, in some cases reaching the solution ratio, with higher uptake observed for the SM with greater hydrogen-bond strength (NCOOH > NOH). The variation in film morphology with solvent and dip-coating rate (spherical for toluene; spherical and cylindrical for *p*-dioxane; spherical, cylindrical, and lamellar for THF; and lamellar only for CHCl₃; for a block copolymer whose equilibrium morphology in the bulk is near the cylindrical/lamellar phase boundary) depends on the initial solution state (whether micellar or not and hardness of micelles) and the SM uptake ratio. These factors, along with solvent evaporation rate and film thickness, influence the kinetics of morphology development in the drying films, the point at which the kinetics are frozen in, the effective block ratio, and the orientation of the morphological structures.



INTRODUCTION

Block copolymer thin films have been intensely investigated in the past two decades due to their nanometer-scale periodicity, making them suitable and versatile substrates for nanomaterial applications in electronics, photovoltaic cells, lithography, photonics, biosensing, etc.^{1–11} The understanding and control of their thin film self-assembly leading to periodic structures continue to present challenges. While being driven by the thermodynamics of block phase separation and interfacial interaction parameters, kinetic processes typically play a significant role in controlling the final film patterns. These processes are highly dependent on the film preparation technique (e.g., spin-coating, dip-coating, blade-coating, annealing procedures, etc.) as well as solvent selectivity and evaporation rate.

Compared to spin-coating, the dip-coating technique for preparing block copolymer films has received limited

attention.^{12–23} However, it is an important industrial technique, offering advantages such as simplicity of use, minimal loss of solution, and ability to coat irregular surfaces.^{24–28} Furthermore, whereas spin-coating of block copolymer films usually requires thermal or solvent annealing to develop various surface nanopatterns, dip-coating typically gives such patterns directly, which can be attributed to effective (though usually partial) solvent annealing during the coating process.²⁰ Dip-coating is also a “softer” technique that does not involve significant viscous stresses on the polymer chains as compared to spin-coating. Importantly, it has been shown recently that very slow dip-coating rates introduce a different coating mechanism compared to higher dip-coating rates (explained below),²⁴

Received: April 21, 2015

Revised: June 16, 2015

which, when combined with supramolecular control, leads to a powerful method for obtaining various nanopatterns from a single dip-coating solution.²³ For all these reasons, the dip-coating of (supramolecular) block copolymer films merits increased attention to better understand and exploit the parameters that influence the film characteristics.

Dip-coating was first modeled for Newtonian liquids by Landau and Levich.²⁹ This model postulates a competition between gravity-induced viscous drag and adhesion of the fluid layer to the substrate and successfully predicts that the film thickness increases with dip-coating rate (withdrawal speed). Grosso and co-workers, in preparing inorganic films from sol-gel solutions, extended the usual lower limit of dip-coating rates (typically 1–10 mm/s) to much lower ones (as low as 0.01 mm/s).^{24,25} They thereby discovered that on decreasing the rate into the latter range the film thickness increases once again, resulting in an overall V-shaped dependence of film thickness on dip-coating rate. A similar dependence was observed for horizontal knife coating of phospholipid films using a receding meniscus technique³⁰ and, more recently, for dip-coating of organic semiconductor films.³¹ The left arm of the V-curve is attributed to convective capillarity feeding of the depositing film due to the solvent evaporation rate being greater than the three-phase drying line displacement.^{24,30} The two arms have been termed capillarity (or capillary) regime and draining regime, respectively.

We showed that the V-shaped thickness–rate dependence also applies to dip-coated block copolymer films,²³ which simultaneously clarified that our preceding work had been conducted in the capillarity regime.^{19–22} This work involved poly(styrene-*b*-4-vinylpyridine) (PS–P4VP) block copolymers mixed in THF with the block-selective small molecules (SM), naphthol (NOH) and naphthoic acid (NCOOH), which can hydrogen bond to P4VP. It was discovered that the SM/VP molar ratio in the dip-coated films (SM uptake) compared to that in solution is very low at the lowest dip-coating rates and increases with rate to reach the solution ratio in the draining regime.^{21,23} This evolution in the supramolecular film composition with dip-coating rate, combined with the thickness evolution, was observed to directly influence the film morphology and surface nanopatterns.^{21,23} Indeed, for PS–P4VP of 30 wt % P4VP, whose equilibrium bulk morphology is near the cylindrical/lamellar phase boundary,³² the film morphology changed with increase in dip-coating rate from spheres to horizontal cylinders and, finally, to vertical cylinders for NOH-containing solutions and up to horizontal lamellae for NCOOH-containing solutions. The changes in morphology were related to increased swelling of the P4VP phase by the SM with increasing SM content in the film,²³ while the morphology orientation can be attributed to film thickness and solvent evaporation rate effects.^{33,34}

The objective of the present contribution is to extend these investigations to other solvents, notably *p*-dioxane, toluene, and chloroform. *p*-Dioxane and chloroform have been used frequently for dip-coating of other supramolecular PS–P4VP films and were shown to give morphologies that are highly dependent on the type of solvent.^{15–18} However, these studies were conducted in the draining regime only, where there is less variation in SM uptake with dip-coating rate (see later). The choice of solvent is also of interest considering that some lead to micellar solutions (THF, *p*-dioxane, and toluene, which are all PS-selective)^{35,36} and others do not (chloroform, which is a good solvent for both PS and P4VP). Furthermore, THF and *p*-

dioxane are hydrogen-bond breakers in that they compete strongly with P4VP as a hydrogen-bond acceptor, whereas toluene and chloroform do not.³⁷ Indeed, preliminary results in a very limited range of the capillarity regime using chloroform indicate that the SM uptake ratio is much higher than in THF (and higher for NCOOH than for NOH) and lead mainly to a lamellar morphology.²² This illustrates that the choice of solvent is an additional crucial parameter that influences the characteristics of supramolecular block copolymer films obtained by dip-coating.

EXPERIMENTAL SECTION

Materials. Poly(styrene-*b*-4-vinylpyridine) (PS–P4VP) copolymers, one with $M_n(\text{PS}) = 41.5 \text{ kg/mol}$, $M_n(\text{P4VP}) = 17.5 \text{ kg/mol}$, and $M_w/M_n(\text{total}) = 1.07$ (referred to as 41.5K–17.5K and used in all experiments except where otherwise specified) and one with $M_n(\text{PS}) = 36.5 \text{ kg/mol}$, $M_n(\text{P4VP}) = 16.0 \text{ kg/mol}$, and $M_w/M_n(\text{total}) = 1.15$ (referred to as 36.5K–16.0K and used for infrared analysis), were purchased from Polymer Source (Dorval, QC) and used as received. 1-Naphthol (NOH, >99%; Sigma-Aldrich), 1-naphthoic acid (NCOOH, 99.8%; Fluka), chloroform (CHCl_3 , 99.99%; VWR), tetrahydrofuran (THF, 99.99%; VWR), toluene (99.9%; Fisher Scientific), and *p*-dioxane (99.0%; EMD Chemicals) were all used as received. Rectangular substrates of $5 \times 10 \text{ mm}^2$ were cut from $\{1,0,0\}$ silicon wafers (University Wafer, Pittsburgh), cleaned by immersion in THF in an ultrasonic bath for 5 min, KimWiped, and dried under nitrogen flow. Subsequently, they were put in a piranha solution at room temperature for 30 min, rinsed with Milli-Q water, and dried under nitrogen flow.

Solution Preparation and Dip-Coating Procedure. Solutions were prepared, unless otherwise noted, by dissolving 50 mg of PS-*b*-P4VP in 5 mL of solvent, giving polymer concentrations of 10 mg/mL, to which was added an equimolar amount of small molecule (SM) relative to VP. CHCl_3 and *p*-dioxane solutions were stirred overnight at room temperature, THF solutions at 40 °C, and toluene solutions at 85 °C. The solutions were then filtered through a 0.45 (and sometimes also a 0.2) μm PTFE filter (Chromspec). Dip-coated films were obtained from these solutions under ambient conditions (~21 °C), using the dip-coater of a KSV3000 Langmuir–Blodgett trough on a vibration-free table (with the beaker of solution placed in the empty trough) or an equivalent stand-alone KSV NIMA dip-coater (KN4001) on an optical table. The silicon substrates were vertically immersed in the solutions at a rate of 5 mm/min, followed by a pause of 30 s, and then were withdrawn at controlled rates between 0.1 and 80 mm/min (referred to as the “dip-coating rate”). The films were left to dry overnight in covered containers at room temperature, unless otherwise indicated. (As explained below, it was necessary to do the infrared analysis within a day of film deposition, whereas this was unimportant for AFM observations and ellipsometry measurements.) In some cases (specified), films were immersed for 1 min in MeOH and then blow-dried with N_2 gas to reveal the morphology.

Light Scattering. Static light scattering (SLS) measurements were performed using a Wyatt Technology DAWN EOS multiangle detector equipped with a 690 nm laser. The solutions were manually injected using a HPLC pump with a 2 mL injection loop at a rate of 0.3 mL/min. Zimm plots were obtained using the ASTRA V.5.3.4.20 software for 6–8 different concentrations of each copolymer solution (ranging from 0.05 to 0.3 mg/mL). The radii of gyration were calculated from the Zimm plots. Dynamic light scattering (DLS) measurements of the 0.3 mg/mL solutions were performed using a Brookhaven BI-200SM instrument equipped with a 532 nm laser (except for the CHCl_3 solutions, for which the Wyatt instrument was used). The measurements were carried out at an angle of 90° and a temperature of 20 °C, controlled by a thermostated circulating water bath. Each hydrodynamic radius was averaged over three measurements whose polydispersity was less than 0.1. Using the system software, the method of cumulants with the third-order model was applied to fit the normalized autocorrelation function.

NMR. Samples for ^1H NMR measurements were prepared by dissolving the desired components in the desired deuterated solvents, at a concentration of about 5 mg/mL. ^1H NMR spectra were measured with a 400 MHz Bruker Avance instrument.

Ellipsometry. Film thicknesses were measured with a M-2000 V spectroscopic ellipsometer (J.A. Woollam) at an angle of 65°, using the Cauchy model to fit the data. Each sample was measured at three different locations to obtain an average. Some film thicknesses were also determined as we did previously,^{20,21,23} based on AFM topography images of scratches of the film down to the substrate surface. They corresponded within 10% to the ellipsometrically determined thicknesses, generally being slightly lower.

Infrared Spectroscopy. Fourier transform attenuated total reflection infrared (ATR-IR) spectra, obtained from an accumulation of 256 interferograms at a resolution of 4 cm⁻¹, were recorded with a Bruker Optics Tensor 27 spectrometer equipped with a MCT (mercury cadmium telluride) detector. A Harrick VariGATR accessory with a hemispherical Ge ATR crystal was used with p-polarized radiation at a 60° incident angle. Calibration plots, obtained with films of 200–300 nm in thickness that were drop-cast onto silicon wafers from PS-P4VP/SM chloroform solutions of known SM/VP molar ratios, were used to quantify the SM/VP uptake ratio in the dip-coated thin films, as described in detail elsewhere.²¹ (Attempts were made to drop-cast films for calibration directly onto the ATR crystal, but this was found to generally overestimate the SM/VP ratio, and thus this method was abandoned.) The bands used for calibration and for determining the SM/VP uptake ratio were 1387 and 1510 cm⁻¹ for NOH and NCOOH, respectively, relative to the PS-P4VP band at 1493 cm⁻¹ (absorbance ratios). It was verified that these bands were not affected by residual solvent bands, except for toluene, which has an absorbance band at 1495 cm⁻¹. In the latter case, the possible presence of solvent was ruled out by the absence of the most intense toluene band at 726 cm⁻¹.) The SM/VP uptake values are estimated to have a general precision of about 5% (up to 10% for the lowest uptake ratios), not considering the issue described in the next paragraph.

It was found that the SM, particularly NOH, tends to evaporate over time from the prepared films; for example, as followed by IR, the NOH content decreased by about 10% and NCOOH by about 2–3% over a 5 h period in films drop-cast onto Si from CHCl₃ solutions. To minimize this problem while still allowing enough time for solvent evaporation (particularly *p*-dioxane and toluene), the infrared spectra of the dip-coated films were taken within a few hours of preparation. Spectra of the drop-cast films for the calibration curves were taken within about 15 min after drop-casting. In our previous publications,^{20,21,23} the calibration spectra were also obtained quickly and the spectra of dip-coated films were generally taken on the same day as dip-coating or, at most, the following day; however, a difference of a few hours in analyzing the dip-coated films might be enough to account for some differences between equivalent data for THF in the present paper and previously. Indeed, it took some time to realize that some irreproducibility in the infrared analysis appeared to be related mainly to SM evaporation, leading us to make a final full analysis using 36.5K–16.0K PS-P4VP, given that insufficient 41.5K–17.5K PS-P4VP remained and was no longer available from the supplier.

Atomic Force Microscopy (AFM). AFM images were obtained in tapping mode using a Digital Instruments Multimode microscope with a Nanoscope V controller, operated under ambient atmosphere, and Nanoworld tips (Arrow-NCR, Al coated, spring constant 42 N/m, oscillation frequency ca. 285 kHz).

Transmission Electron Microscopy (TEM). Cross-sectional TEM images were taken with a Philips Tecnai 12 operated at an acceleration voltage of 80 kV. The dip-coated films were first coated with a layer of carbon using a Cressington carbon coater (4.8 V, 6 s). They were then covered with epoxy resin (Embed-812, Electron Microscopy Sciences) and cured at 60 °C for 36 h. Next, the films were peeled off the silicon substrate after immersion in liquid nitrogen for 30 s.³⁷ The recovered film was embedded in epoxy in a mold form and cured at 60 °C for 36 h. The cured epoxy-embedded films were microtomed across the film plane into slices of approximately 70–80 nm thick, using a Reichert-Jung Ultracut E microtome equipped with a

Drukker diamond knife. Finally, the slices were deposited on Formvar–carbon-coated copper TEM grids (Mecalab) and exposed for 3 h to I₂ vapor.

RESULTS AND DISCUSSION

Effect of Solvent on the Film Thickness vs Dip-Coating Rate Relation. It is known that various parameters, including dip-coating rate (withdrawal speed), solution concentration, and temperature, have a strong influence on film thickness in the dip-coating process, until recently studied almost exclusively in the draining regime.^{24,26,38–40} The nature of the solvent is an additional important parameter affecting the film thickness,^{41–43} and we want to determine how this parameter influences the recently discovered V-shaped relation between film thickness and dip-coating rate covering both the capillarity and draining regimes.

Figure 1 compares these plots for solutions of THF, toluene, *p*-dioxane, and CHCl₃ containing 10 mg/mL of PS-P4VP and

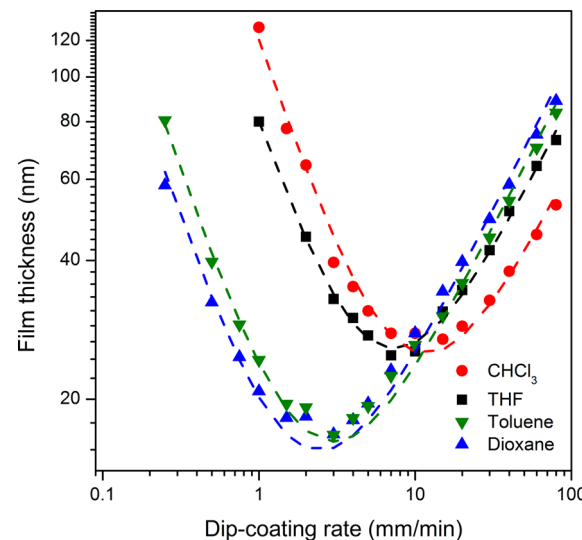


Figure 1. Film thickness as a function of dip-coating rate (withdrawal speed) from NCOOH-containing solutions of PS-P4VP (10 mg/mL copolymer concentration, equimolar NCOOH:VP). The dashed curves are plotted according to eq 1,²⁴ using the fitting constants given in Table 1 (see text for details).

equimolar NCOOH. The data confirm that the film thickness varies with dip-coating rate in a V-shaped manner in all cases. These measurements were not done systematically with the corresponding NOH-containing or SM-free solutions, but our previous results in THF indicate that the type (NCOOH or NOH) or absence of SM has no discernible influence on the curve.^{20,23} However, increasing the polymer concentration in solution, and therefore k_i , displaces the overall curve vertically,^{23,24} as confirmed also for CHCl₃ solutions (Figure SI-2 in the Supporting Information).

The dashed curves in Figure 1 represent fits to the four sets of data using eq 1, a semiempirical equation given in ref 24 to model the combined capillarity and draining regimes (the latter derived from the Landau–Levich equation^{24,29}). According to this equation, the dried film thickness, h_0 , varies with dip-coating rate (withdrawal speed), u , as u^{-1} in the capillarity regime and $u^{2/3}$ in the draining regime, as follows:

$$h_0 = k_i \left(\frac{E}{L} u^{-1} + D u^{2/3} \right) \quad (1)$$

where k_i is a material proportion constant, E the solvent evaporation rate, L the width of the film (typically the same as the substrate used), and D a global constant related to the physicochemical properties of the solution (fluid).²⁴

The material proportion constant, k_i , allows an estimation of the theoretical dried film thickness (the original equation being in terms of the deposited wet film), by taking it as equal to c_i/ρ_i where c_i is the solution concentration and ρ_i is the density of the dried material.^{24,31} Since both c_i and ρ_i , and therefore k_i , in the current systems vary (details in the Supporting Information), due to the variation in SM content in the films with solvent and dip-coating rate, as will be shown later, we chose to include k_i with the two prefactors, E/L and D , for fitting the data in Figure 1 by eq 1. These values—determined by a linear regression procedure with normalization by the film thickness, using the Excel solver add-in (and generally within 10% of the values determined by the procedure used in ref 24; see Figure SI-1 and Table SI-1 in the Supporting Information)—along with the minimum thickness, h_{\min} , and the corresponding dip-coating speed, u_c , given by the fits, are tabulated in Table 1.

Table 1. Prefactors ($k_i E/L$, $k_i D$) for Eq 1, Used To Fit the Data in Figure 1, and Resulting Dip-Coating Speed (u_c) at Minimum Film Thickness (h_{\min})

| solvent | $k_i E/L$ ($10^{-12} \text{ m}^2 \text{ s}^{-1}$) | $k_i D$ ($10^{-6} \text{ m}^{1/3} \text{ s}^{2/3}$) | u_c (mm min ⁻¹) | h_{\min} (nm) |
|-------------------|--|--|----------------------------------|--------------------|
| THF | 1.3 | 6.2 | 7.4 | 25.7 |
| p-dioxane | 0.25 | 7.9 | 2.4 | 15.5 |
| toluene | 0.32 | 7.2 | 3.0 | 16.2 |
| CHCl ₃ | 2.0 | 4.5 | 11.7 | 25.1 |

Figure 1 and Table 1 show that the minimum in the curves occurs at distinctly different film thicknesses and dip-coating rates, depending on the solvent. They are higher for THF and CHCl₃ at about 25–26 nm and 7–12 mm/min and lower for p-dioxane and toluene at about 16 nm and 2–3 mm/min. In parallel, the draining side of the V-curve is similar for all four solvents, whereas the capillarity side is displaced to significantly lower dip-coating rates for p-dioxane and toluene than for THF and CHCl₃. The displacement of the capillarity regime means that the draining regime extends to lower dip-coating rates for p-dioxane and toluene, allowing the films to continue to decrease in thickness with decrease in dip-coating rate until the capillarity regime sets in and becomes dominant.

To understand the V-curve displacements, it is useful to review the changes observed and discussed in ref 24 for sol–gel films dip-coated at different sample chamber temperatures. There, it was shown that temperature has no significant influence on the film thickness in the draining regime, whereas

an increase in temperature leads to an increase in thickness in the capillarity regime (resulting also in an increase in the critical dip-coating rate and film thickness of the V-curve minimum). The invariance in the draining regime was attributed to a balancing out of opposing influences of increased temperature, thus leaving the parameter D essentially unchanged; that is, at a higher temperature, the resulting lower viscosity leads to a decrease in film thickness whereas the resulting higher solvent evaporation rate (lower surface tension) allows less time for viscous drag on the liquid film, leading to an increase in film thickness. In the capillarity regime, on the other hand, greater evaporation due to higher temperature increases the rate of capillarity feeding at the drying line (reflected by an increase in the value of E/L with temperature), leading to thicker films. Thus, with increasing temperature, the influence of the capillarity regime extends to higher dip-coating rates, with a concomitant increase in critical thickness and rate for the V-curve minimum.

These explanations for the temperature effect can be applied to the solvent effect observed in Figure 1, noting also that the much smaller influence of dip-coating solvent in the draining regime compared to the capillarity regime is similar to the temperature effect. Despite the minimal effect of the solvent in the draining regime, small differences are detectable, with the film thickness at a constant dip-coating rate decreasing in the order *p*-dioxane > toluene > THF > CHCl₃ (or the opposite for the dip-coating rate at a constant film thickness). A correlation can be made with the prefactor K of the Landau–Levich equation for a nonevaporating Newtonian fluid, $h = Ku^{2/3}$, expressed as^{24,29}

$$K = \frac{0.94\eta^{2/3}}{\gamma^{1/6}(\rho g)^{1/2}} \quad (2)$$

where η , γ , and ρ are the fluid viscosity, surface tension and density, respectively, of the solution and g is the gravitational force. This prefactor for the entrained fluid film is the equivalent of the prefactor, $k_i D$, in eq 1 for the dry film (neglecting evaporation-dependent parameters).²⁴ To determine the relative trend in K for the different solutions, it suffices to use the values of η , γ , and ρ for the pure solvents (Table 2). The resulting relative K are given in Table 2, and it is observed that K decreases in the same order as the film thickness for the different solvents (and also follows the same order as the $k_i D$ values in Table 1). This can be taken to rationalize the trend observed in the draining regime.

In the capillarity regime, the dominant influence is the rate of evaporation, as indicated above for the temperature effect, determined primarily by the solvent vapor pressure. As shown in Table 2, the vapor pressures of *p*-dioxane and toluene, relatively similar, are much lower than those of THF and CHCl₃, which are also relatively similar. This qualitatively rationalizes the difference in the capillarity regime between these two pairs of solvents, where the much lower volatility of

Table 2. Physical Characteristics of the Solvents Used and the Prefactor K^a

| | vapor pressure (kPa) | viscosity (mPa·s) | surface tension (mN m ⁻¹) | density (g mL ⁻¹) | K ($10^{-4} \text{ m}^{1/3} \text{ s}^{2/3}$) |
|-------------------|----------------------|-------------------|---------------------------------------|-------------------------------|---|
| tetrahydrofuran | 21.6 | 0.456 | 26.50 ^b | 0.883 | 1.10 |
| <i>p</i> -dioxane | 4.95 | 1.177 | 32.75 | 1.027 ^c | 1.85 |
| toluene | 3.79 | 0.560 | 27.73 | 0.862 | 1.26 |
| chloroform | 26.2 | 0.537 | 26.67 | 1.479 | 0.94 |

^aAt 25 °C and from ref 44 unless otherwise specified. K is calculated from these values using eq 2 (see text for details). ^bFrom ref 45. ^cFrom ref 46.

p-dioxane and toluene shifts the capillarity regime to lower dip-coating rates. In other words, for the latter solvents, one must dip-coat at lower speeds to reach the point where the solvent evaporation rate becomes faster than the dip-coating rate, the condition that defines the capillarity regime. It is noteworthy that while the order of film thickness at a constant dip-coating rate (and the order of dip-coating rate at a constant film thickness) in the capillarity regime is $\text{CHCl}_3 > \text{THF} \gg \text{toluene} > p\text{-dioxane}$, the order of vapor pressure is $\text{CHCl}_3 > \text{THF} \gg p\text{-dioxane} > \text{toluene}$. The inversion in the order of *p*-dioxane and toluene suggests perhaps that the viscosity, which is much higher for *p*-dioxane compared to the other three solvents (Table 2), might also have some influence on the capillarity regime by reducing the effectiveness or kinetics of capillary feeding of the depositing film, thereby resulting in a thinner film.

The above indicates that the primary influences governing the differences in the V-curves in Figure 1 are related to the solvent characteristics. Whether the solution is micellar or not appears to have no significant effect. This is shown by the THF and CHCl_3 solutions, which are micellar and nonmicellar, respectively (see the next section), yet give similar V-curves due to their similar solvent characteristics in contrast to the other two solvents.

State of SM-VP Hydrogen Bonding in Solution.

Hydrogen bonding in solution can be probed by NMR.³⁷ Table 3 lists the chemical shifts of the NOH and NCOOH

Table 3. ^1H NMR Chemical Shift of the Hydroxyl Proton of NOH and NCOOH in Deuterated Solvents before and after Addition of PS-P4VP or Pyridine (Equimolar SM:VP or SM:Pyridine)

| solvent | chemical shift (ppm) | | | |
|-------------------|----------------------|-------------------------------|--------------------|-----------------------------------|
| | NOH | PS-P4VP/NOH (pyridine/NOH) | NCOOH | PS-P4VP/NCOOH (pyridine/NCOOH) |
| THF | 8.86 | 8.89 | 11.50 ^a | 11.5 ^a |
| <i>p</i> -dioxane | 8.29 | 8.32 | 10.88 ^a | 10.8 ^a |
| toluene | 4.35 | 4.75 ^a (7.90) | NS | NS (11.84) |
| chloroform | 5.26 | NS ^b (9.40) | NS | NS (11.65) |

^aVery broad with very low intensity (Figure SI-3) ^bNS = no signal found.

hydroxyl proton, in the absence and presence of PS-P4VP (1:1 SM:VP), in the deuterated forms of the four solvents used. Examining NOH first, the chemical shift of the hydroxyl proton in THF and *p*-dioxane is unchanged by the addition of PS-P4VP, whereas in toluene there is a downfield displacement from 4.35 to 4.76 ppm accompanied by a large reduction in intensity and increase in broadness (Figure SI-3) but no change in relative integration. In CDCl_3 , the OH signal, located at 5.26 ppm in the absence of PS-P4VP, is no longer found after addition of PS-P4VP. For an analogous CDCl_3 solution of NOH and equimolar pyridine, in contrast, a signal appears at 9.40 ppm (accompanied by the disappearance of the signal at 5.26 ppm). Similar observations regarding the OH chemical shift displacements in different solvents were made by Huang et al.³⁷ for 3-pentadecylphenol (PDP) solutions in the absence and presence of PS-P4VP; i.e., they reported that there are no chemical shift displacements in oxygen-bearing solvents like THF and *p*-dioxane and moderate downfield displacements ranging from 0.3 to 0.6 ppm in non-oxygen-bearing solvents

like toluene and CDCl_3 (visible in their case for the latter solvent).

The downfield displacement caused by PS-P4VP (or pyridine) in CDCl_3 and toluene is ascribed, as in ref 37, to SM-VP H-bonding taking place in these two nonpolar solvents. The invariability of the chemical shift in THF and *p*-dioxane is indicative of the competition of the polar solvent molecules for the SM H-bond due to the H-bond accepting oxygen atom; thus, in these two solvents, H-bonding with the solvent overwhelms SM-VP H-bonding and is thus unaffected by the presence or not of PS-P4VP.

The stronger H-bond donor, NCOOH, similarly shows no NMR displacement of the acid proton signal in THF and *p*-dioxane (Table 3). It may be noted that this signal is broad for NCOOH alone in these solvents and even broader for NCOOH in the presence of PS-P4VP (Figure SI-3). In toluene and CDCl_3 , this signal is not visible at all either for NCOOH alone or in the presence of PS-P4VP but is found at 11.6–11.8 when equimolar pyridine is added in place of the polymer (Table 3). Thus, no conclusions can be drawn concerning any signal displacement in these two solvents. It is noteworthy that the magnitude of the displacements for NOH and NCOOH H-bonded to the solvent or to pyridine is high (7.9–9.4 for NOH, 10.9–11.8 for NCOOH), whereas, as shown for NOH in toluene here and for PDP in several solvents in ref 37, it is much lower in nonpolar solvents and when H-bonded to P4VP.

State of Micellization in Solution. It is known that PS-P4VP diblock copolymers form micellar solutions in THF, toluene, and *p*-dioxane due to the insolubility of the P4VP block in these solvents^{35,36,47} (except for low molecular weight P4VP in THF), whereas CHCl_3 , as a good solvent for both blocks, does not lead to micellar solutions.⁴⁸ In the context of the present study and given literature reports that small molecules that are hydrogen-bonded to one of the blocks can alter the solubility behavior of block copolymers,^{17,48–51} it is of interest to determine if the addition of NOH or NCOOH has an influence on the micellar characteristics and how the micellar rigidity varies among the solvents. This was addressed by static and dynamic light scattering (SLS and DLS) experiments to obtain the radii of gyration, R_g , and the hydrodynamic radii, R_h , respectively. Previously, we found that in THF the presence of either SM has no detectable influence on the size and shape of the micelles, since the R_g and R_h values and their ratios show no significant change.²⁰ The data given in Table 4 indicate that this

Table 4. Hydrodynamic Radius (R_h) and Radius of Gyration (R_g) of PS-P4VP in the Solvents Used, with and without the Presence of SM (NOH or NCOOH, Equimolar SM:VP)

| solvent | sample | R_g (nm) | R_h ^a (nm) | R_g/R_h |
|-------------------|-----------------|----------------|-------------------------|-----------|
| THF ^b | PS-P4VP | 19.2 ± 4.8 | 27.1 | 0.71 |
| | PS-P4VP + NOH | 19.1 ± 4.2 | 26.4 | 0.72 |
| | PS-P4VP + NCOOH | 19.6 ± 2.8 | 26.2 | 0.75 |
| <i>p</i> -dioxane | PS-P4VP | 25.2 ± 0.9 | 35.6 | 0.71 |
| | PS-P4VP + NOH | 25.0 ± 0.5 | 35.7 | 0.70 |
| | PS-P4VP + NCOOH | 25.2 ± 0.5 | 35.6 | 0.71 |
| toluene | PS-P4VP | 32.5 ± 0.8 | 52.6 | 0.62 |
| | PS-P4VP + NOH | 31.9 ± 0.4 | 51.8 | 0.62 |
| | PS-P4VP + NCOOH | 32.6 ± 0.6 | 52.7 | 0.62 |

^aPDI < 0.1; $R_h = 8.6\text{--}9.0$ nm in CHCl_3 (with and without SM).

^bFrom ref 20.

is the same for the *p*-dioxane (shown also by Gohy and co-workers using 2-hydroxy-6-naphthoic acid⁵²) and toluene micellar solutions as well as for CHCl₃ solutions. For the latter, the R_h values are ca. 9 nm whether or not SM is present, which is close to the estimated value for single flexible chains (ca. 8 nm), thus indicating that the CHCl₃ solutions are not micellar.

For the micellar solutions, the R_g/R_h ratios in *p*-dioxane and toluene, like in THF,²⁰ are always less than 0.775, which is considered to be the upper limiting value for spherical micelles whose core is much denser than the shell.^{35,53} It is noteworthy that the R_g/R_h ratios in the three solvents, averaged over the solutions with and without the SM, vary in the order THF (0.73) > *p*-dioxane (0.71) > toluene (0.62) (the difference between THF and *p*-dioxane may be within experimental uncertainty). This can be correlated with an increase in hardness of the micelle cores due to decreasing solvent swelling of the micellar core.^{29,34} Thus, the micelle cores are relatively soft in THF and *p*-dioxane (due to partial swelling by the solvent) and harder in toluene. The decrease in solvent swelling correlates in turn with increasingly unfavorable interactions between the solvent and P4VP. The latter also favors larger micelles, according to the trends in the R_g and R_h values, which go as toluene > *p*-dioxane > THF.

The relative mobility in the micellar cores can be probed directly by ¹H NMR by comparison of appropriate P4VP signals. Figure 2 shows the NMR spectra of pure PS-P4VP in

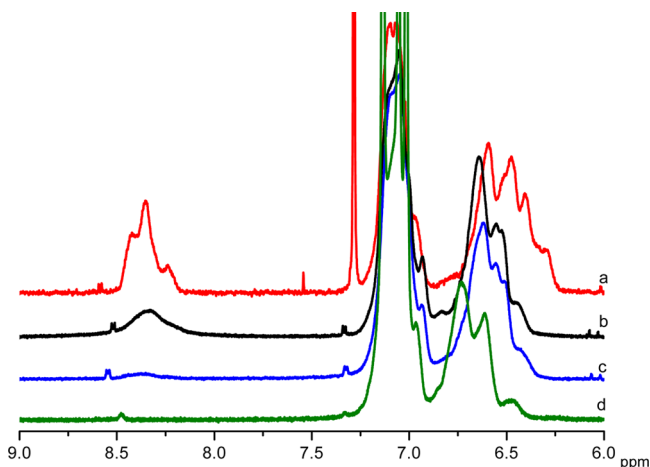


Figure 2. Partial ¹H NMR spectra of pure PS-P4VP block copolymer in (a) CDCl₃, (b) THF-*d*₈, (c) *p*-dioxane-*d*₈, and (d) toluene-*d*₈.

the four deuterated solvents in the region of the pyridine aromatic protons vicinal to the nitrogen atom (8.2–8.5 ppm), normalized approximately to the PS proton signals at 6.9–7.2 ppm. Clearly, the signal is most intense and best resolved in CDCl₃, consistent with the good solubility and therefore mobility of the P4VP block in this solvent. It appears as a single, broad signal with reduced intensity in THF and much reduced intensity in *p*-dioxane, reflecting decreasing mobility. In toluene, it is essentially absent, indicative of a glassy core.⁴⁷ The order of the decrease in intensity and mobility parallels the trend indicated above for the R_g/R_h ratios (this time with a clear difference between THF and *p*-dioxane), reflecting increasing hardness of the cores due to decreasing solvent content.

Effect of Solvent on the Small Molecule Uptake in Dip-Coated Films.

As mentioned above, we had found that when using THF as solvent, the SM content in the films relative to that in the dip-coating solution (SM/VP uptake ratio), determined by infrared spectroscopy, increases with the dip-coating rate in the capillarity regime, starting from a very low ratio and reaching that of the solution composition in the draining regime where it remains approximately constant.²³ The behavior in the capillarity regime was rationalized by the extraction or washing out of a fraction of the SM from the depositing film during capillary feeding, where the solution meniscus is in contact with the depositing film while solvent is evaporating (giving a three-phase contact line); in this case, the longer the contact time (i.e., the slower the dip-coating rate), the more effectively SM is washed out. This (partial) SM extraction was thought to be facilitated by the absence of (or minimal) SM-VP H-bonding in THF, due to the latter's property as a competitive H-bond acceptor. In the draining regime, in contrast, the fluid film, maintained by adsorption to the substrate, is pulled out of the dip-coating solution, leaving little or no time for SM extraction.

The evolution of the SM/VP uptake ratio with dip-coating rate for equimolar NOH- and NCOOH-containing solutions for the other three solvents, in comparison with THF, is shown in Figure 3. These data were obtained using a different

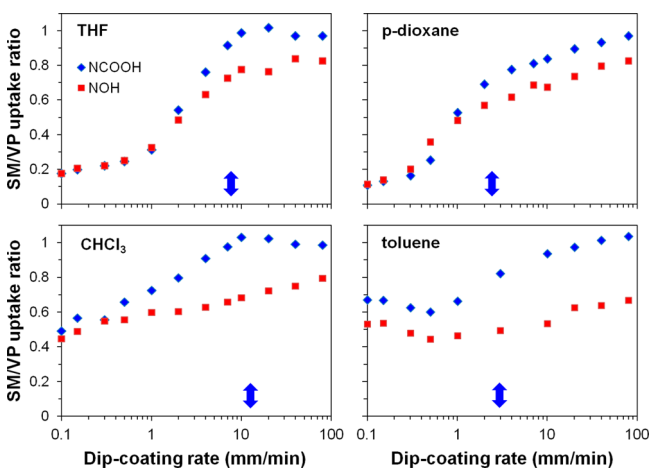


Figure 3. Evolution of SM/VP uptake ratio with dip-coating rate in PS-P4VP (36.5K–16K)/SM films dip-coated from the solutions indicated (10 mg/mL copolymer concentration, SM/VP = 1). The arrow indicates the rate giving the minimum film thickness (u_c in Table 1).

copolymer, 36.5K–16.0K, having a block ratio very similar to the 41.5K–17.5K used above (30.5 vs 29.7 wt % P4VP, with a small difference also in total molecular weight). (The R_h values determined with this copolymer, with commentary, are given in Table SI-2 and generally follow the trends observed in Table 4.) Overall, the uptake ratios tend to increase with dip-coating rate, and there is a tendency for the curves to have a sigmoidal shape, particularly in THF and *p*-dioxane, with the steepest rise occurring near the film thickness minimum on the capillarity side (less clear for both SMs in toluene and for NOH in CHCl₃).

However, there are distinct differences among the different solvents. For the two H-bond competitive solvents, THF and *p*-dioxane, the uptake ratio starts from lower values (0.1–0.2) compared to the other two solvents (0.4–0.7) at the lowest

Table 5. Morphologies in Dip-Coated Films Using Different Solvents, in Relation to Relevant Properties

| | THF ^a | <i>p</i> -dioxane | toluene | CHCl ₃ |
|---------------------------------|--|---|---------------------------|-------------------|
| <i>properties</i> | | | | |
| block selectivity | PS-selective ^b | PS-selective ^b | PS-selective ^b | nonselective |
| micellar property | soft core | less soft core | rigid core | nonmicellar |
| H-bond competitor ^c | strong | strong | weak | weak |
| SM uptake ^d | low to high | low to high | medium to high | medium to high |
| <i>morphologies^e</i> | | | | |
| pure PS-P4VP | sph | sph | sph | lam |
| PS-P4VP/NOH | sph $\xrightarrow{(5-10)}$ cyl (h) $\xrightarrow{(20-40)}$ cyl (v) | sph $\xrightarrow{(20-30)}$ cyl (v) | sph | lam |
| PS-P4VP/NCOOH | sph $\xrightarrow{(\sim 2)}$ cyl (h) $\xrightarrow{(\sim 20)}$ lam | sph $\xrightarrow{(2-5)}$ cyl (h) $\xrightarrow{(20-30)}$ cyl (h + v) | sph | lam |

^aMorphology evolutions shown in ref 23. ^bThe selectivity of the solvent for PS relative to P4VP (and therefore the micelle core rigidity) increases in the order THF < *p*-dioxane < toluene. ^cRefers to the competition of the solvent molecules with VP as a hydrogen-bond acceptor. ^dIn general, the SM/VP uptake ratio is lower in the capillarity regime (lower dip-coating rates) and higher in the draining regime (higher dip-coating rates); it increases more or less gradually, depending on the solvent, with increase in dip-coating rate. NOH uptake appears to be a little lower than NCOOH uptake, especially in the draining regime and with toluene and CHCl₃. ^eMorphologies: sph = spherical, cyl = cylindrical, lam = lamellar. Morphology changes are given in order of dip-coating rate, with the boundaries given by the rates indicated above the arrows (mm/min). The final morphologies are strongly influenced by the micellar core rigidity in solution (the more rigid the micelle core, the sooner the evolving morphologies are kinetically arrested during solvent evaporation) and by the SM uptake in the films (the SMs being P4VP-selective, thereby increasing the P4VP + SM volume fraction). Cylinder orientation (h = horizontal; v = vertical) relative to the substrate typically depends on film thickness and solvent evaporation rate.^{33,34}

dip-coating rate investigated (0.1 mm/min). Furthermore, for NOH in THF, the plateau reached in the draining regime lies at about 0.8 instead of equimolar as reported previously (see Experimental Section).²³ For *p*-dioxane, the uptake ratio starts at slightly lower values than for THF and rises more gradually as the draining regime sets in reaching equimolar for the NCOOH-containing solution only at the highest rate used (80 mm/min). In both cases, the uptake ratios are about the same in the capillarity regime for NOH- and NCOOH-containing solutions, whereas in the draining regime, those for the NOH-containing solutions are 10–20% lower than those for the NCOOH-containing solutions.

For CHCl₃ and toluene solutions, the variation in uptake ratio with dip-coating rate is smaller due to the higher values at low dip-coating rates, but the difference between NOH- and NCOOH-containing solutions is greater than for THF and *p*-dioxane solutions, particularly for toluene. Except for the higher starting point, the uptake ratio for NCOOH-containing CHCl₃ solutions varies similarly to those for THF, reaching a plateau at equimolar near the thickness minimum, whereas those for NOH-containing CHCl₃ solutions rise approximately linearly from about 0.45 to 0.8 over the dip-coating rate range studied. For toluene solutions containing NOH, the uptake ratio varies even less with dip-coating rate, from about 0.5 to 0.6–0.7, whereas for NCOOH in toluene, the uptake ratio in the capillarity regime is about 0.6–0.7 and then gradually rises as the draining regime sets in, reaching equimolar at the highest dip-coating rates (an apparent shallow minimum at 0.5 mm/min may or may not be real).

The large difference in the lower limits of uptake ratio for THF and *p*-dioxane compared to CHCl₃ and toluene can be related to the fact that the former are H-bond competitors whereas the latter are not; i.e., the washing out of SM in the capillarity regime mentioned above is less effective in solvents where there is significant SM–P4VP hydrogen bonding. Indeed, the tendency to a lower limit plateau in the capillarity regime might reflect an equilibrium in each solution between SM that is H-bonded to P4VP and SM that is free or H-bonded to solvent molecules. Moreover, the stronger H-bond between NCOOH and P4VP compared to NOH and P4VP²⁰ can be

expected to lead to a higher H-bond fraction for NCOOH, which can thus rationalize its tendency to lead to higher uptake ratios than NOH in CHCl₃ and toluene solutions in the capillarity regime. The greater NCOOH than NOH uptake in the draining regime for all four solutions, particularly CHCl₃ and toluene, is possibly related in part to NOH evaporation in the few hours between sample preparation and IR measurements (it is estimated that this could account for a difference of up to 10–15%; see the Experimental Section). There might also be a relation with the fact that a fraction of the NOH in the dry film is dispersed in the PS phase,²¹ where it is not retained by H-bonding, and this fraction might be subject to drainage during dip-coating. It should be added that in the final dried films P4VP shows H-bonding to an extent that is consistent with the uptake ratios, as found before for THF solutions.^{20,21}

Consequences on Dip-Coated Film Morphologies.

The final film morphologies in the dried films dip-coated from the four types of solutions are anticipated to be strongly influenced by the foregoing properties. These properties are summarized for each solvent in the first part of Table 5, where the block selectivity determines the micellar property, and the degree of the H-bond competitiveness of the solvent combined with the dip-coating regime (capillarity versus draining) strongly influences the SM uptake in the films. The film thickness, which varies with dip-coating rate, is also an important factor for film morphologies.

The morphologies deduced from AFM and complementary cross-sectional TEM images—described hereafter—are summarized in the second part of Table 5 as a guide for what follows. It is to be noted that dip-coating from SM-free PS-P4VP solutions that are micellar give films characterized by a surface pattern of dots, suggestive of spherical morphologies (ref 23 for THF, Figure SI-4 for *p*-dioxane) that are kinetically trapped from the micellar solutions. This morphology is confirmed by a cross-sectional TEM image of a film dip-coated from a THF solution (Figure SI-5). The morphologies of films dip-coated from SM-containing solutions are more variable, depending on the solvent used, the dip-coating rate, and the type of SM. This is described next for each type of solution,

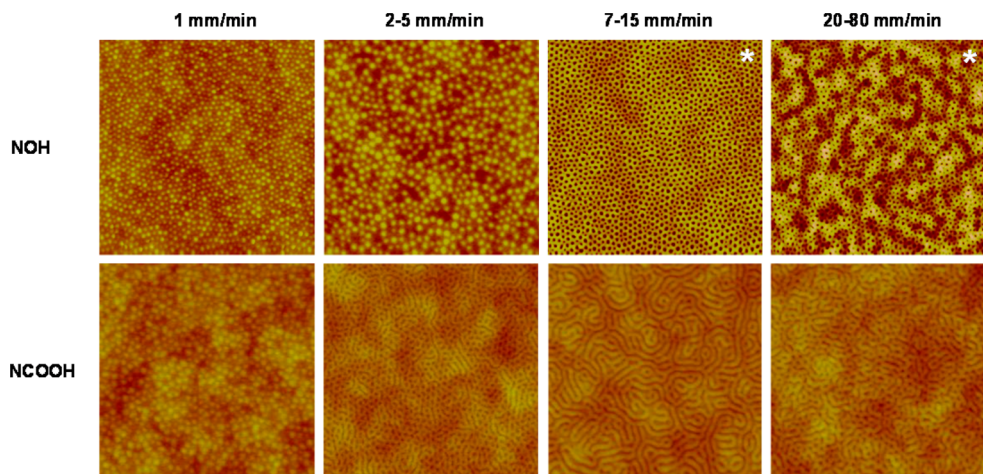


Figure 4. Representative AFM height images ($2 \times 2 \mu\text{m}^2$) of PS–P4VP films dip-coated from SM-containing *p*-dioxane solutions (10 mg/mL copolymer concentration) at the rates indicated. Images designated with an asterisk are of samples immersed briefly in methanol.

followed by morphology–property correlations that rationalize the trends observed in the different solvents.

THF Solutions. Dip-coating from NOH-containing THF solutions has been observed previously²³ to give surface patterns that evolve with increasing dip-coating rate from dots, to mixed dots and short stripes, to long stripes, to a second region of mixed dots and short stripes, to predominantly dots. This was interpreted as an evolution from a spherical morphology to a cylindrical morphology with first horizontal and then vertical orientation of the cylinders relative to the film plane, with the mixed patterns attributed to boundary regions between two morphologies. This evolution can be attributed to the increased swelling of the P4VP/NOH phase due to increasing NOH content (as indicated by the uptake ratio data), along with the influence^{33,34} of solvent evaporation rate and film thickness on the cylinder orientation. Similarly, for films dip-coated from NCOOH-containing THF solutions over the same dip-coating range, the surface pattern evolves from dots, to mixed dots and short stripes, to long stripes, to islands-and-holes, interpreted as an evolution from P4VP/NCOOH spherical micelles to horizontal cylinders to flat-on lamellae. The evolution up to a lamellar morphology for NCOOH but not for NOH was ascribed to almost complete selectivity of NCOOH for the P4VP phase, compared to a small fraction of NOH dispersed in the PS phase (as indicated by DSC measurements²¹). Thus, it was presumed that the somewhat greater volume fraction of the NCOOH/P4VP phase compared to the NOH/P4VP phase is (just) enough for the system to enter the lamellar phase for NCOOH, but not (quite) enough for NOH. From the uptake ratios shown in Figure 3 for a slightly different copolymer in THF, it appears that somewhat less NOH than NCOOH is taken up in the draining regime, which would then also contribute to the difference in their morphological evolution at the higher dip-coating rates (although, if due mainly to some NOH loss due to evaporation from the film, as discussed above, the final morphology may already be frozen in before most loss occurs).

***p*-Dioxane Solutions.** Similar trends are observed with *p*-dioxane solutions, with the main difference that the morphology evolution with dip-coating rate is more limited compared to THF solutions. For NOH-containing solutions, the AFM topographic images (Figure 4) show that only the dot pattern is observed whatever the dip-coating rate. [Note that

for dip-coating rates of 10 mm/min and above the as-dip-coated films appeared featureless, and the dot pattern (in the form of pores) was revealed by brief rinsing in methanol, which washes out the SM and spreads out some of the P4VP over the surface,^{15,16,19} leaving behind nanoporous thin films.] Assuming a spherical morphology at the lowest dip-coating rates where the SM/VP uptake ratio is low (and therefore compositionally similar to the SM-free films), the invariance of the dot pattern can imply either no change in the spherical morphology up to the highest dip-coating rates used or an undetected change from spherical to vertical cylindrical morphology.

To distinguish between the two possibilities, a cross-sectional TEM micrograph (Figure 5a) was obtained from I₂-stained slices of a PS–P4VP/NOH film dip-coated at a rate of 40 mm/min from the *p*-dioxane solution. Despite some deformation of the slice and the irregular presence of the carbon coating (the very dark regions, on the air side of the original film), the

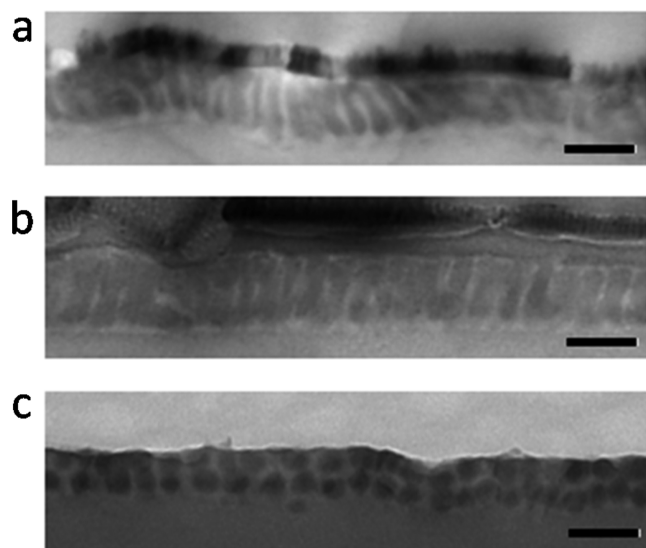


Figure 5. TEM micrographs of cross-sectional slices of carbon-coated and I₂-stained PS–P4VP/SM thin films obtained by dip-coating at 40 mm/min (draining regime) from (a) NOH/*p*-dioxane, (b) NCOOH/*p*-dioxane, and (c) NCOOH/toluene solutions. The substrate is located in the bottom part of the images. Scale bars = 100 nm.

micrograph shows clearly that vertical P4VP-based cylinders (gray-colored) traverse the PS matrix (light-colored). The absence of horizontal cylinders in the thinner films (in the vicinity of the thickness minimum at 2–3 mm/min dip-coating rate) suggests that the transition to cylindrical morphology occurs in a higher dip-coating range where the films are thick enough to favor vertical cylinders, deduced to be around 20–30 mm/min. It may be added here that the vertical cylinders may have formed by a mechanism involving the vertical coalescence of spheres due to out-of-plane film shrinkage during solvent evaporation, as proposed by Stamm and co-workers for PS–P4VP films (10 wt % P4VP) containing nominally equimolar 2-(4'-hydroxyphenylazo)benzoic acid (HABA) that were vapor annealed by *p*-dioxane.^{15,16,54}

For NCOOH-containing *p*-dioxane solutions, the surface morphology was observed to evolve with increasing dip-coating rate from dots, to mixed dots and short stripes, to long stripes, to another mixed dot-and-stripe region. This is consistent with an evolution from a spherical morphology, to a transition region of mixed spheres and horizontal cylinders, to a pure cylindrical morphology where the cylinders are first oriented horizontally (7–15 mm/min where the films are near the thickness minimum) and then both horizontally and vertically. A TEM micrograph of a cross-sectional slice of a film dip-coated at 40 mm/min is shown in Figure 5b. For this film, only one piece was successfully retrieved, and the TEM image shows that this piece is characterized by vertical P4VP-based cylinders (gray-colored) like for the NOH-containing film. It may also be noticed that there appears to be a horizontal cylinder below the carbon layer (air side of the original film). At the least, this micrograph shows that vertical cylinders are present in the film in the region of the dot-and-stripe pattern. The persistence over a rather wide range of dip-coating rates (20–80 mm/min) of the mixed dot-and-stripe region, suggestive of mixed horizontal and vertical cylindrical structures, might be related to the slower evaporation rate of *p*-dioxane compared to THF, leading to a less pronounced solvent concentration gradient during solvent evaporation. According to ref 33, a sharp solvent concentration gradient leads to perpendicular cylinders, whereas a weak one leads to horizontal cylinders. In the case of the NCOOH-containing *p*-dioxane solutions, it is possible that an intermediate situation occurs, such that neither horizontal nor vertical orientation is strongly favored at the film thicknesses involved.

In summary for films dip-coated from *p*-dioxane solutions, the morphology evolution is attenuated compared to films dip-coated from THF solutions. This is particularly evident by the fact that the NCOOH system does not evolve up to the lamellar morphology for *p*-dioxane (as it does for THF) even at the highest dip-coating rate where the SM uptake is the same in both solvents. It is also observed that at least for NOH-containing solutions, the spherical morphology transforms into the cylindrical morphology at dip-coating rates that are higher for *p*-dioxane than for THF (Table 5), although this may be related, at least in part, to the more gradual rise in SM uptake ratio in this dip-coating range for *p*-dioxane compared to THF solutions (Figure 3). On the other hand, like for THF, NOH-containing *p*-dioxane solutions lead to a slower morphology evolution than NCOOH-containing solutions (20–30 vs 2–5 mm/min for the spherical/cylindrical boundary), which can again be rationalized by the more complete selectivity of NCOOH for the P4VP phase, possibly combined with the

somewhat higher NCOOH uptake ratios for dip-coating rates in the draining regime.

Toluene Solutions. For films prepared from toluene solutions, the surface pattern of dots was observed for both NOH and NCOOH for all dip-coating rates (Figure 6). [Films

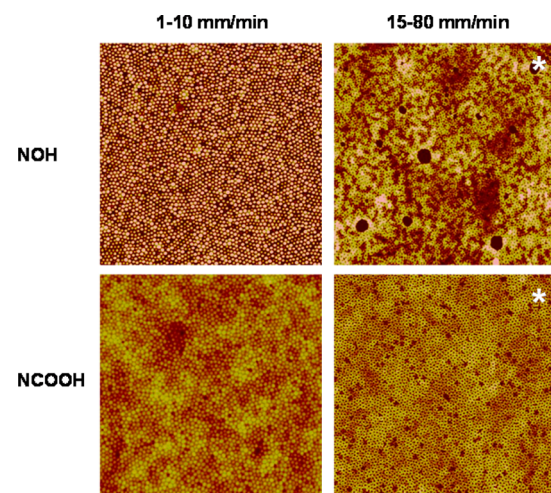


Figure 6. Representative AFM height images ($4 \times 4 \mu\text{m}^2$) of PS–P4VP films dip-coated from SM-containing toluene solutions (10 mg/mL copolymer concentration) at the rates indicated. Images designated with an asterisk are of samples immersed briefly in methanol.

dip-coated in the draining region (about 15 mm/min and above) were initially featureless, this time for both SMs, and required rinsing in MeOH to reveal the pattern in the form of pores.] The cross-sectional TEM micrograph of a NCOOH-containing film dip-coated at 40 mm/min (Figure 5c, noting that the carbon layer became detached from the film during microtoming and is therefore not observed, although it was visible as a separate piece in a larger-scale TEM image) shows P4VP-based spheres in a PS matrix. Thus, it can be concluded that the morphology remains spherical at least up to 40 mm/min (if not throughout the entire dip-coating range investigated).

Chloroform Solutions. All of the films dip-coated from CHCl_3 solutions, including SM-free ones (Figure SI-4), are characterized by an “islands-and-holes” surface morphology (Figure 7), typical of the face-down lamellar morphology in the form of terraces due to incommensurability between the film thickness and the natural periodicity of the block copolymer.^{22,55} [Note that these films were dip-coated from more dilute solution than for the other solvents; however, as shown in ref 23 for THF solutions, this is highly unlikely to change the morphology, although it shifts the curve of average film thickness versus dip-coating rate downward and thus can affect the distribution of islands and holes.] This is related, of course, to the fact that CHCl_3 is a common solvent for the PS and P4VP blocks (and for the SM), as will be further commented on in the next section. It may be noticed that for the lowest dip-coating rates (1–2 mm/min), which are also where the thickest films are obtained, some stripes appear in the NOH-containing thin films; these might be vertically oriented lamellae or perhaps cracks that appear in the last stage of drying.

Property–Morphology Correlations. The different morphology evolutions in the different solvents must be understood considering the initial state of the solution and the

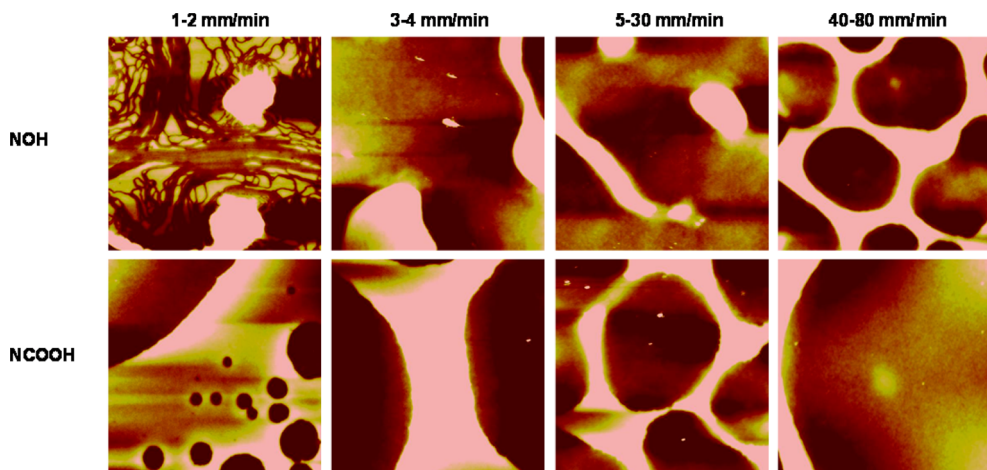


Figure 7. Representative AFM height images ($10 \times 10 \mu\text{m}^2$) of PS–P4VP films dip-coated from SM-containing chloroform solutions (copolymer concentration 5 mg/mL) at the rates indicated.

solvent distribution between the PS- and P4VP-based phases during solvent evaporation from the deposited wet film until immobility sets in while also taking into account the SM uptake, which is predominantly sequestered in the P4VP phase. The more equal the solvent distribution between the two blocks is, the closer the final morphology will be to the equilibrium melt morphology in the bulk. The latter is the case for CHCl_3 , which, as a nonselective solvent that is good for both blocks, leads to molecularly dispersed solutions initially. As solvent evaporates from the wet film, phase separation eventually takes place with concomitant morphology development. During the evaporation process, CHCl_3 remains distributed roughly proportionally between the PS and P4VP(/SM) phases while keeping both mobile (i.e., plasticized) to high concentration. On the block copolymer phase diagram, this can be visualized as moving vertically upward from the disordered region into the ordered (lamellar) region. The variation in SM uptake does not affect the morphology, since even the SM-free solution leads to lamellar morphology, which can be understood from the fact that the equilibrium bulk morphology of the copolymer used is near the cylindrical/lamellar boundary,³² and because the addition of the SM up to equimolar SM/VP leads to a P4VP/SM volume fraction at about midpoint in the composition range for (equilibrium) lamellar morphology.

The general perspective for the PS-selective solvents (THF, *p*-dioxane, toluene), which give micellar solutions, is that the greater the PS selectivity is, the further the starting point of morphology evolution during solvent evaporation is to the left of the effective phase diagram (in terms of the P4VP(/SM) block fraction where it is assumed that solvent is included in the partitioning into effective block volume fractions). This, combined with increased rigidity of the P4VP-based micellar core due to decreased solvent content (also resulting from greater PS selectivity), causes immobility to set in sooner as the solvent evaporates, and consequently, the final morphology is closer to the initial micellar solution morphology and, in parallel, farther from the equilibrium bulk morphology. Expressed in another way, solvent located in the micellar core helps maintain mobility to a greater degree of film dryness, thereby allowing the morphology of the drying film to evolve further along the pathway that starts from the (spherical) micellar morphology and ends with the equilibrium dry-film

lamellar morphology. When the mobility becomes insufficient, the evolution along the pathway is arrested (sooner or later depending on the solvent), resulting in frozen-in kinetic morphologies. Superimposed on the effect of solvent on morphology evolution during solvent evaporation is the effect of SM uptake that increases the volume fraction of the P4VP-based phase. In addition, the SM contributes to mobility in the P4VP phase by adding free volume, particularly at low solvent content (at high solvent content, the effect of the solvent is overwhelming).

Specifically, the morphological starting point for the three micellar solutions are all spherical, but in order, from left to right on the phase diagram, as toluene → *p*-dioxane → THF. This follows from the NMR data (Figure 2) and R_g/R_h ratios (Table 4) indicating that the order of the P4VP core mobility is THF > *p*-dioxane > toluene, the last being essentially immobile on the NMR time scale. Without any SM present, the frozen-in morphologies in the dried films are also all spherical (even those dip-coated from THF where the micellar cores are softest and therefore susceptible to the greatest evolution as the film is drying), indicating that chain immobility sets in during solvent evaporation before the system has time to cross a morphological boundary. The addition of P4VP-selective SM, by increasing the P4VP-based phase volume fraction (and its mobility), allows morphological evolution across boundaries to take place. How this evolution depends on the solvent is most clearly observed at the highest dip-coating rates for NCOOH, where the SM/VP molar uptake in the films is equimolar (with essentially all of the NCOOH confined to the P4VP phase), and therefore the P4VP/NCOOH volume fraction is the same, for all three solvents. The morphology achieved, which is observed to be lamellar, cylindrical, and spherical for THF, *p*-dioxane, and toluene, respectively, reflects the decrease in mobility of the P4VP-based core from THF to *p*-dioxane to toluene. It is particularly noteworthy that even with equimolar SM content in the films, there is no crossing of boundaries for the toluene solutions; i.e., the initial micellar (spherical) morphology is conserved. This is attributed to the glassiness of the micelle cores that is not compensated for by the high SM content. In other words, of the three solutions, the morphology in the films dip-coated from toluene solutions is the furthest from the equilibrium bulk morphology. For *p*-dioxane and THF solutions, the SM uptake ratio determines where the final

frozen-in morphology lies between the extremes observed for SM-free films (spherical), on the one hand, and for films containing equimolar NCOOH in the P4VP phase (cylindrical for *p*-dioxane, lamellar for THF), on the other hand. The further fact that NCOOH is more selective than NOH for the P4VP phase and the observation that the NOH uptake ratio tends to be a little lower than the NCOOH uptake ratio accounts for the differences observed between these two SMs in each solvent. Finally, it should be added that in these analyses the possibility of gyroid phases was neglected for simplicity, although some of the apparently mixed surface patterns might be related to such phases.

In summary, the morphology evolution in the dip-coated thin films can be rationalized considering the micellar properties of the solutions (determined by the block selectivity of the solvent) and the SM content in the films. Obviously, the morphologies and their evolution can be further manipulated by changing the block copolymer composition (block fraction and type), modifying the small molecule (nature of non-covalent bond, molecular weight, shape, concentration), using other solvents as well as mixed solvents, changing the temperature, etc. This thus represents a facile technique for generating various useful surface nanopatterns.

CONCLUSIONS

A variety of surface patterns can be achieved through dip-coating of supramolecular block copolymer solutions of a single composition using different solvents. This contribution has shown that a PS-P4VP diblock copolymer with a minority P4VP block, whose equilibrium bulk morphology is near the cylindrical/lamellar phase boundary, can give rise to surface patterns based on morphologies ranging from spherical to lamellar when dip-coated from solutions containing an equimolar quantity of a P4VP-selective small molecule. The film morphology and hence surface pattern achieved depend on the block selectivity of the solvent, the SM uptake (which determines the effective block ratio), and the film thickness (which, along with solvent evaporation rate, influences the phase structure orientation). The film thickness has a V-shaped dependence on the dip-coating rate, with a minimum that is highly dependent on the solvent vapor pressure, due primarily to lower volatility displacing the capillarity regime (low dip-coating rate side of the V-curve) to lower dip-coating rates. The SM uptake is also dependent on the dip-coating rate, tending to rise with increasing rate, but with a starting point that is much lower for solvents that are strong hydrogen-bond competitors of P4VP, which is ascribed to a washing-out effect in the capillarity regime. The solvent block selectivity has a dominating influence on the morphology by its influence on the initial solution structure and, when micellar, on the rigidity of the micelle core. Thus, nonselective solvents like CHCl₃ lead to a morphology (lamellar here) that is closest to the expected equilibrium morphology in the bulk, whereas PS-selective solvents lead to morphologies that range from the initial solution morphology (spherical) to somewhere along the pathway toward the equilibrium morphology. The more PS-selective the solvent is—i.e., the less solvent present in the micellar core and therefore the more rigid the core—the closer the final (kinetically frozen-in) film morphology is to the initial micellar morphology. In accordance with this and as supported by NMR and light scattering data, the micellar mobility in the solvents parallels the maximum degree of morphological

evolution in the order THF (up to lamellar with NCOOH) > *p*-dioxane (up to cylindrical) > toluene (spherical only).

ASSOCIATED CONTENT

Supporting Information

Data-fitting details for Figure 1 and Table 1, other thickness vs dip-coating rate curves, NMR spectra, radii of gyration for the 36.5K–16.0K system, AFM images of films dip-coated from SM-free *p*-dioxane and CHCl₃ solutions, cross-sectional TEM image of a film dip-coated from an SM-free THF solution. The Supporting Information is available free of charge on the ACS Publications website at DOI: 10.1021/acs.macromol.5b00847.

AUTHOR INFORMATION

Corresponding Authors

*E-mail: geraldine.bazuin@umontreal.ca (C.G.B.).

*E-mail: re.prudhomme@umontreal.ca (R.E.P.).

*E-mail: c.pellerin@umontreal.ca (C.P.).

Notes

The authors declare no competing financial interest.

ACKNOWLEDGMENTS

The research was funded by the Natural Sciences and Engineering Research Council (NSERC) of Canada and le Fonds de Recherche du Québec - Nature et Technologies (FRQ-NT). The authors thank Prof. Antonio Nanci, Dr. Rima Wazen, and Katia J. Ponce of the Faculté de médecine dentaire of Université de Montréal for access to the instrumentation for and assistance with obtaining the cross-sectional TEM results.

REFERENCES

- (1) Kim, H.-C.; Park, S.-M.; Hinsberg, W. D. *Chem. Rev.* **2010**, *110*, 146–177.
- (2) Bang, J.; Jeong, U.; Ryu, D. Y.; Russell, T. P.; Hawker, C. J. *Adv. Mater.* **2009**, *21*, 4769–4792.
- (3) Segalman, R. A. *Mater. Sci. Eng., R* **2005**, *48*, 191–226.
- (4) Fasolka, M. J.; Mayes, A. M. *Annu. Rev. Mater. Res.* **2001**, *31*, 323–355.
- (5) Li, M.; Coenjarts, C. A.; Ober, C. K. *Adv. Polym. Sci.* **2005**, *190*, 183–226.
- (6) Hamley, I. W. *Prog. Polym. Sci.* **2009**, *34*, 1161–1210.
- (7) Marencic, A. P.; Register, R. A. *Annu. Rev. Chem. Biomol. Eng.* **2010**, *1*, 277–297.
- (8) Kim, J. K.; Yang, S. Y.; Lee, Y.; Kim, Y. *Prog. Polym. Sci.* **2010**, *35*, 1325–1349.
- (9) Galatsis, K.; Wang, K. L.; Ozkan, M.; Ozkan, C. S.; Huang, Y.; Chang, J. P.; Monbouquette, H. G.; Chen, Y.; Nealey, P.; Botros, Y. *Adv. Mater.* **2010**, *22*, 769–778.
- (10) Sinturel, C.; Vayer, M.; Morris, M.; Hillmyer, M. A. *Macromolecules* **2013**, *46*, 5399–5415.
- (11) Luo, M.; Epps, T. H. *Macromolecules* **2013**, *46*, 7567–7579.
- (12) Meiners, J. C.; Ritzi, A.; Rafailovich, M. H.; Sokolov, J.; Mlynek, J.; Krausch, G. *Appl. Phys. A: Mater. Sci. Process.* **1995**, *61*, 519–524.
- (13) Li, Z.; Zhao, W.; Liu, Y.; Rafailovich, M. H.; Sokolov, J.; Khougaz, K.; Eisenberg, A.; Lennox, R. B.; Krausch, G. *J. Am. Chem. Soc.* **1996**, *118*, 10892–10893.
- (14) Meiners, J. C.; Quintel-Ritzi, A.; Mlynek, J.; Elbs, H.; Krausch, G. *Macromolecules* **1997**, *30*, 4945–4951.
- (15) Sidorenko, A.; Tokarev, I.; Minko, S.; Stamm, M. *J. Am. Chem. Soc.* **2003**, *125*, 12211–12216.
- (16) Tokarev, I.; Krenek, R.; Burkov, Y.; Schmeisser, D.; Sidorenko, A.; Minko, S.; Stamm, M. *Macromolecules* **2005**, *38*, 507–516.
- (17) Nandan, B.; Vyas, M. K.; Böhme, M.; Stamm, M. *Macromolecules* **2010**, *43*, 2463–2473.

- (18) Kuila, B. K.; Gowd, E. B.; Stamm, M. *Macromolecules* **2010**, *43*, 7713–7721.
- (19) Laforgue, A.; Bazuin, C. G.; Prud'homme, R. E. *Macromolecules* **2006**, *39*, 6473–6482.
- (20) Roland, S.; Gaspard, D.; Prud'homme, R. E.; Bazuin, C. G. *Macromolecules* **2012**, *45*, 5463–5476.
- (21) Roland, S.; Pellerin, C.; Bazuin, C. G.; Prud'homme, R. E. *Macromolecules* **2012**, *45*, 7964–7972.
- (22) Roland, S.; Prud'homme, R. E.; Bazuin, C. G. *Sci. China: Chem.* **2013**, *S6*, 33–39.
- (23) Roland, S.; Prud'homme, R. E.; Bazuin, C. G. *ACS Macro Lett.* **2012**, *1*, 973–976.
- (24) Faustini, M.; Louis, B.; Albouy, P. A.; Kuemmel, M.; Grossi, D. *J. Phys. Chem. C* **2010**, *114*, 7637–7645.
- (25) Grossi, D. *J. Mater. Chem.* **2011**, *21*, 17033–17038.
- (26) Yimsiri, P.; Mackley, M. R. *Chem. Eng. Sci.* **2006**, *61*, 3496–3505.
- (27) Faustini, M.; Boissière, C.; Nicole, L.; Grossi, D. *Chem. Mater.* **2014**, *26*, 709–723.
- (28) Faustini, M.; Ceratti, D. R.; Louis, B.; Boudot, M.; Albouy, P.-A.; Boissière, C.; Grossi, D. *ACS Appl. Mater. Interfaces* **2014**, *6*, 17102–17110.
- (29) Landau, L.; Levich, B. *Acta Phys. Chim. U. R. S. S.* **1942**, *17*, 42–54.
- (30) Le Berre, M. I.; Chen, Y.; Baigl, D. *Langmuir* **2009**, *25*, 2554–2557.
- (31) Li, L.; Gao, P.; Wang, W.; Müllen, K.; Fuchs, H.; Chi, L. *Angew. Chem., Int. Ed.* **2013**, *52*, 12530–12535.
- (32) Ruokolainen, J.; Saariaho, M.; Ikkala, O.; ten Brinke, G.; Thomas, E. L.; Torkkeli, M.; Serimaa, R. *Macromolecules* **1999**, *32*, 1152–1158.
- (33) Phillip, W. A.; Hillmyer, M. A.; Cussler, E. L. *Macromolecules* **2010**, *43*, 7763–7770.
- (34) Morikawa, Y.; Nagano, S.; Watanabe, K.; Kamata, K.; Iyoda, T.; Seki, T. *Adv. Mater.* **2006**, *18*, 883–886.
- (35) Antonietti, M.; Heinz, S.; Schmidt, M.; Rosenauer, C. *Macromolecules* **1994**, *27*, 3276–3281.
- (36) Förster, S.; Zisenis, M.; Wenz, E.; Antonietti, M. *J. Chem. Phys.* **1996**, *104*, 9956–9970.
- (37) Huang, W.-H.; Chen, P.-Y.; Tung, S.-H. *Macromolecules* **2012**, *45*, 1562–1569.
- (38) Kuznetsov, A. V.; Xiong, M. *Int. Commun. Heat Mass Transfer* **2002**, *29*, 35–44.
- (39) Huang, L. C.; Richman, E. K.; Kirsch, B. L.; Tolbert, S. H. *Microporous Mesoporous Mater.* **2006**, *96*, 341–349.
- (40) Lee, C. H.; Lu, Y. F.; Shen, A. Q. *Phys. Fluids* **2006**, *18*, 052105.
- (41) Brinker, C. J.; Hurd, A. J. *J. Phys. III* **1994**, *4*, 1231–1242.
- (42) Hurd, A. J. In *The Colloid Chemistry of Silica*; American Chemical Society: Washington, DC, 1994; Vol. 234, pp 433–450.
- (43) Jung, B. G.; Min, S.-H.; Kwon, C.-W.; Park, S.-H.; Kim, K.-B.; Yoon, T.-S. *J. Electrochem. Soc.* **2009**, *156*, K86–K90.
- (44) Haynes, W. M. *CRC Handbook of Chemistry and Physics*, 95th ed.; CRC Press: Boca Raton, FL, 2014.
- (45) Dean, J. A. *Lange's Handbook of Chemistry*, 15th ed.; McGraw-Hill: New York, 1999.
- (46) Brandrup, J.; Immergut, E. H.; Grulke, E. A.; Abe, A.; Bloch, D. R. *Polymer Handbook*, 4th ed.; John Wiley & Sons: New York, 1999.
- (47) Riess, G. *Prog. Polym. Sci.* **2003**, *28*, 1107–1170.
- (48) Peng, H.; Chen, D.; Jiang, M. *Langmuir* **2003**, *19*, 10989–10992.
- (49) van Zoelen, W.; Polushkin, E.; ten Brinke, G. *Macromolecules* **2008**, *41*, 8807–8814.
- (50) Yao, X.; Chen, D.; Jiang, M. *J. Phys. Chem. B* **2004**, *108*, 5225–5229.
- (51) Yao, X.; Chen, D.; Jiang, M. *Macromolecules* **2004**, *37*, 4211–4217.
- (52) Bharatiya, B.; Schumers, J.-M.; Poggi, E.; Gohy, J.-F. *Polymers* **2013**, *5*, 679–695.
- (53) Antonietti, M.; Bremser, W.; Schmidt, M. *Macromolecules* **1990**, *23*, 3796–3805.
- (54) Böhme, M.; Kuila, B.; Schlörb, H.; Nandan, B.; Stamm, M. *Phys. Status Solidi B* **2010**, *247*, 2458–2469.
- (55) Kim, S.; Nealey, P. F.; Bates, F. S. *ACS Macro Lett.* **2012**, *1*, 11–14.